Damage accumulation in Si during high-dose self-ion implantation

Y. Zhong, C. Bailat, and R. S. Averback
Department of Materials Science and Engineering, University of Illinois at Urbana Champaign, Urbana, Illinois 61801

S. K. Ghose and I. K. Robinson
Department of Physics, University of Illinois at Urbana Champaign, Urbana, Illinois 61801

(Received 4 December 2003; accepted 28 April 2004)

Accumulation and annealing of damage in Si implanted with self-ions to high doses were investigated using a combination of grazing incidence diffuse x-ray scattering, high-resolution x-ray diffraction scans, and transmission electron microscopy. During implantation at 100 °C, small vacancy and interstitial clusters formed at low doses, but their concentrations saturated after a dose of $\approx 3\times10^{14}$ cm^{-2}. The concentration of Frenkel defects at this stage of the implantation was $\approx 1\times10^{-3}$. At doses above 1×10^{15} cm^{-2}, the concentration of implanted interstitial atoms began to exceed the Frenkel pair concentration, causing the interstitial clusters to grow, and by $\approx 3\times10^{15}$ cm^{-2}, these clusters formed dislocation loops. Kinematical analysis of the rocking curves illustrated that at doses above 1×10^{15} cm^{-2} the "plus one" model was well obeyed, with one interstitial atom being added to the dislocation loops for every implanted Si atom. Measurements of Huang scattering during isochronal annealing showed that annealing was substantial below 700 °C for the specimens irradiated to lower doses, but that little annealing occurred in the other samples owing to the large imbalance between interstitial and vacancy defects. Between 700 and 900 °C a large increase in the size of the interstitial clusters was observed, particularly in the low-dose samples. Above 900 °C, the interstitial clusters annealed. © *2004 American Institute of Physics*. [DOI: 10.1063/1.1763242]

I. INTRODUCTION

Ion implantation has evolved over the past 50 years as an important processing step in the fabrication of numerous semiconductor devices. Since these devices generally require perfect crystalline structures, the issues of defect creation and defect annealing have always been of great concern. In recent years these issues have taken on far greater technological significance since the reduction in the dimensions of the devices has substantially reduced tolerances for diffusion processes, and hence the allowable annealing temperatures. For this reason a great number of investigations on defect mobilities and defect reactions in Si have been undertaken. Indeed, much is now known from a host of spectroscopic techniques and theoretical calculations about the mobilities of point defects in Si and their trapping at various impurities[1]. Despite these advances, it is notable that reconciliation of high temperature diffusion data with defect mobilities deduced from low temperature irradiation experiments remains an unsolved problem.[2–4] For most ion implantations, however, the mobilities and interactions of isolated defects are less crucial for understanding the damage state during annealing than are the properties and structures of point defect clusters. This is a consequence of most implantations being performed with heavy ions, which produce defects in high concentrations in energetic displacement cascades. In such situations, particularly at high doses when cascades overlap, the defects tend to be highly clustered.

Some attempts have been made to investigate the structure and properties of defect clusters in irradiated Si. Most of such investigations have employed transmission electron microscopy (TEM) to study these defect clusters after high temperature annealing,[5] however, TEM only becomes useful after the defects have condensed into dislocation loops. Deep level transient spectroscopy (DLTS) has also been a particularly useful method for studying defects in semiconductors and it has been used to study the evolution of the defect structure from point defects to clusters and finally to extended defects. In one study, for example, Si was implanted with self-ions at energies between 145 keV and 2 MeV, to doses ranging between 1×10^{8}, and 5×10^{13} cm^{-2}, and defect reactions were subsequently monitored during annealing in the range 100–680 °C.[6] DLTS is most useful, however, for studying small defect clusters where known spectroscopic signatures are available. This method, moreover, provides little information about the concentrations of the clusters.

The present work complements past defect studies on ion implanted Si by examining the high-dose implantation regime, $>1\times10^{14}$ cm^{-2}, where the defect populations are comprised almost entirely of defect clusters. We examine here the build up of defect clusters during implantation with self-ions at $\approx$100 °C and subsequently the evolution of the clusters during annealing. In this work we employ Huang diffuse x-ray scattering (HDS) and high-resolution x-ray diffraction scans (HRXRD), in combination with TEM measurements, to provide quantitative information about the structure of defect clusters and their annealing properties.

II. EXPERIMENTAL PROCEDURES

The measurements were performed on Si(111) wafers (resistivity of 100 Ω cm) that were chemically cleaned and

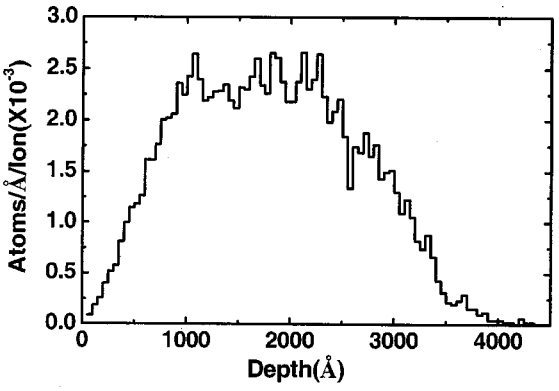

FIG. 1. Si ion distribution in Si, calculated using program TRIM. The dose ratios for the ions with energies of 50 keV, 100 keV, and 150 keV are 1:2:3.

preannealed at 1000 °C prior to implantation with Si ions. The self-ion implantations were carried out using three ion energies, 50 keV, 100 keV, and 150 keV in the ratio 1:2:3 in order to obtain a homogeneous implantation profile over a broad region, as illustrated by the results of simulations shown in Fig. 1. The specimen temperature was maintained at 100 °C during the irradiations to prevent amorphization at these high doses.[7]

Since the penetration of x rays is much greater than that of self-ions at the energies employed here, the use of grazing incidence geometry for HDS was required to minimize the background diffuse scattering from undamaged regions of the sample.[8] The present measurements were performed using the National Synchrotron Light Source (NSLS) at Brookhaven National Laboratory (BNL), beamline X-16A which was developed for surface science.[9] The x-ray measurements were performed on each sample at room temperature before and after each annealing step. The scans were chosen along the radial direction of a {111} reflection. The angle of incidence was fixed at $\approx 1°$. The isochronal annealing was performed on each sample in temperature sequence from low to high by passing a dc current through the sample, with holding times of ≈ 2 min at each temperature. The relation between temperature and applied power was calibrated using an optical pyrometer at high temperatures and a thermocouple welded to a reference sample at low temperatures.

For each specimen, the HDS intensity arising from defects was obtained by point-wise subtraction of the background contributions arising from thermal diffuse scattering, Compton scattering and the Bragg tail. This background intensity was obtained by measuring the scattering intensity after complete annealing of the defects at high temperatures. Measurements on samples cleaved from the same wafer but neither irradiated nor annealed gave similar background intensities.

The theoretical aspects of HDS for defect studies are well described in the literature.[10,11] Additional information about using HDS in grazing incidence geometry and in particular for defects in Si can be found elsewhere.[12–14] The salient points of HDS in regards to the present study can be summarized as follows.

(i) Huang scattering refers to the diffuse scattering intensity close to a reciprocal lattice vector, i.e., small values of q, where $\mathbf{q}=\mathbf{Q}-\mathbf{G};\mathbf{Q}$ is the total scattering vector and $\mathbf{G}$ is the nearest reciprocal lattice vector.
(ii) The scattering intensity is proportional to q^{-2} in the case of point like type defects (Huang scattering) and to q^{-4} in the case of large clusters and dislocation loops (asymptotic scattering).
(iii) The scattering intensity depends on the square of the number of defects in the cluster in the Huang regime, while it depends linearly on this number in the asymptotic scattering regime.
(iv) The crossover point between the -2 and -4 behaviors is determined by the cluster size.

HRXRD measurements of the out of plane lattice parameter, or strain, were performed using the Philips Xpert triple-axis system in the Center for Materials Research (CMM) at UIUC. Measurements of the lattice parameter have long been employed to determine defect concentrations in crystalline materials, as they offer great accuracy, nearly one part in 10^6. Since the relaxation volume of a point defect is ~ 1 atomic volume, Ω_o, these measurements are sensitive to defect concentrations of $\sim 10^{-6}$ atom fraction.

Irradiation of bulk samples with ion beams creates inhomogeneous damage, which complicates the analysis of strain. Nevertheless, a sufficiently uniform strain is generated that well-defined features have been observed in HRXRD in a number of previous experiments on Si (Refs. 15–20), GaAs (Refs. 17 and 21), and Ge.[17] A shifted second peak in the HRXRD scan was detected,[17] then explained for the GaAs case with a dynamical calculation which gave a reasonably good fit.[17] Details of a computer program optimized to carry out these calculations were later provided by Pesek *et al.*[20] A much simpler, alternative dynamical approach based on a single phase parameter was proposed and demonstrated by Tsai *et al.*[15,16] A more detailed description of the dynamical simulation of the rocking curves can be found in Bowen and Tanner's book.[22] Our approach differs from all of these in that it is purely kinematical, based on the idea of crystal truncation rods (CTR),[23] which allows the semi-infinite bulk and the strained surface layers to be modeled together. The kinematical approach is bound to fail at the exact Bragg condition (where a CTR diverges), but away from this condition the absorption length is about six times smaller than the dynamical extinction length that we consider the method to be valid. The details of our method are described in the Appendix. Because the calculation is kinematical, it is a simple linear superposition, which lends itself readily to least-squares fitting as we show. The ability to fit the rocking curves and extract parameters, as well as extract an absolute value for the total (integrated) strain, is the characteristic of our method.

Finally TEM observations were performed to complement the DXS and HRXRD measurements. They provided

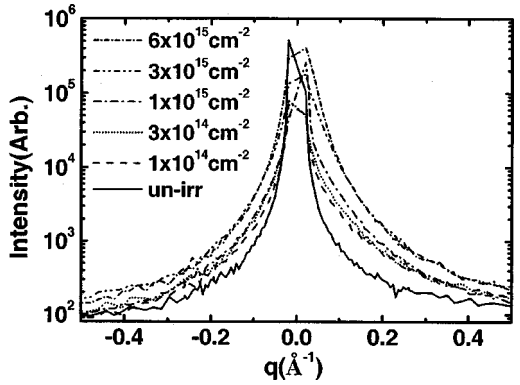

FIG. 2. Typical DXS measurements: intensity as a function of momentum transfer q for samples irradiated at various doses.

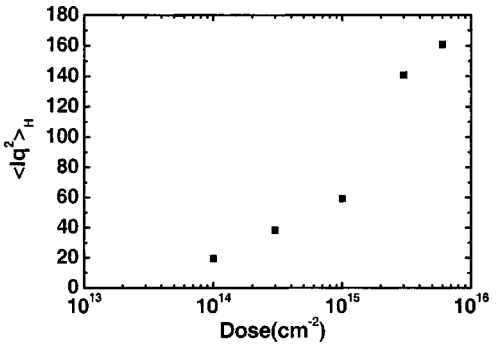

FIG. 4. Average Iq^2, $\langle Iq^2\rangle_H$, as a function of ion dose. The average was obtained by integrating Iq^2 over the q range where HDS is valid.

information about the defect clusters once they formed dislocations. This information is valuable for establishing reference points for the x-ray methods.

III. EXPERIMENTAL RESULTS

A. Evolution of the defect structure during implantation at 100 °C

Typical HDS measurements are shown in Fig. 2, where the measured diffuse scattering intensity is plotted as a function of q for Si doses in the range $0.1-6.0\times10^{15}$ cm^{-2}. The curves are clearly asymmetric, having a higher intensity at positive q. This asymmetry is typical when interstitial rather than vacancy defects dominate the scattering, either because the interstitials have higher concentrations or because they are in larger clusters.[10,11,14] The symmetric (Huang) diffuse HDS is shown in Fig. 3 as a function of q in a log-log plot. The behavior is rather complex, however, we obtain the Huang scattering by averaging Iq^2 over the region where I varies as q^{-2}. Deviation from q^{-2} behavior at small q derives from spatial correlations in the defect concentrations.[11] In the present situation, these correlations presumably arise from the precipitation reactions of interstitial and vacancy defects, i.e., when clusters nucleate, they drain the immediate vicinity of mobile defects. At large values of q, the Huang approximation also breaks down for large clusters, and the asymptotic scattering (q^{-4}) dominates, as noted above. The increase in the size of the clusters with increasing dose is noticeable in Fig. 3 by the shift in the transition from asymptotic to Huang scattering at progressively smaller values of q.

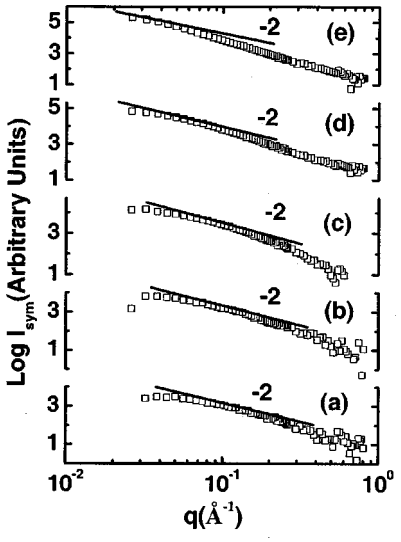

FIG. 3. Symmetric HDS intensity as a function of momentum, transfer q in log-log plot for samples implanted to various doses (a) 1×10^{14}/cm^2, (b) 3×10^{14}/cm^2, (c) 1×10^{15}/cm^2, (d) 3×10^{15}/cm^2, (e) 6×10^{15}/cm^2. The solid lines show the relation of slope −2.

The Huang scattering, $\langle Iq^2\rangle$, is plotted as a function of dose in Fig. 4. It increases slowly, approximately logarithmically, with ion dose at low doses, $\phi<1\text{x}10^{15}$ cm^{-2}, but then it increases far more strongly with dose. The values of $\langle Iq^2\rangle$ shown at the two high doses, moreover, are likely to underestimate the actual Huang scattering, since the region showing a q^{-2} dependence (see Fig. 3) has shifted to very small values of q, where the scattering is reduced by correlation effects. Nevertheless, a clear transition in the dose dependence of Iq^2 occurs at $\approx1\times10^{15}$ cm^{-2}, suggesting a possible change in the defect structure and/or concentration at higher doses.

The results for the HRXRD measurements are plotted as discrete points in Fig. 5(a). Clear oscillations are seen on the low q side of the (333) Bragg peak which develop strongly with dose. The broadening seen was far greater than the effects of wafer curvature, which was measured by translating the sample. Fits to the data using Eq. (A2) from the kinematical model described in the Appendix are represented in Fig. 5(a) by solid lines. The strain profiles deduced from the fitting are shown in Fig. 5(b) and the integral strain is shown in Fig. 5(c) as a function of fluence. Similar to the HDS measurements, the dependence of integrated strain with dose shows two regimes, one at low doses ($\leqslant10^{15}$ cm^{-2}), regime I, and one at high doses ($\geqslant10^{15}$ cm^{-2}), regime II. The strain in the high-dose regime increases approximately linearly with dose.

Lastly we show in Fig. 6 a TEM bright field image obtained from a cross section of the sample irradiated to a dose of 3×10^{15} cm^{-2}. A clear band of damage is seen in the image. The damage consists of point defects that have collapsed into dislocations since point defects and small, uncollapsed defect clusters do not create sufficient strain to be imaged in the TEM under the conditions employed. The surface region,

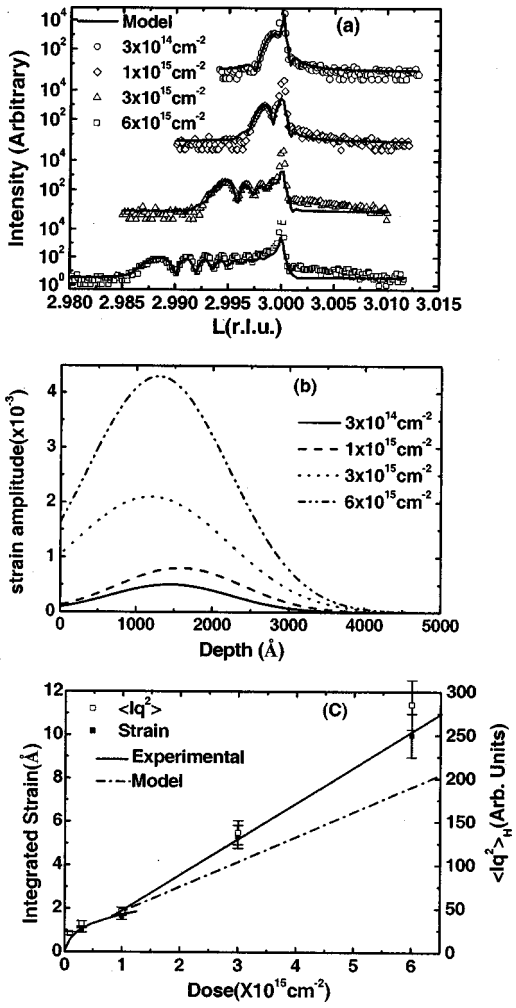

FIG. 5. (a) Strain measurements for samples with various doses. Symbols are for the experimental data and the solid lines are from the fitting. (b) The strain profiles used in the fittings in (a). (c) Integrated strain (solid symbol) as a function of dose. Also shown in the figure are the average Iq^2 (open symbol) of HDS measurements as a function of dose. The solid line is the fit to the HDS experiment data, while the dotted-dashed line is based on the model of the linear superposition of strain.

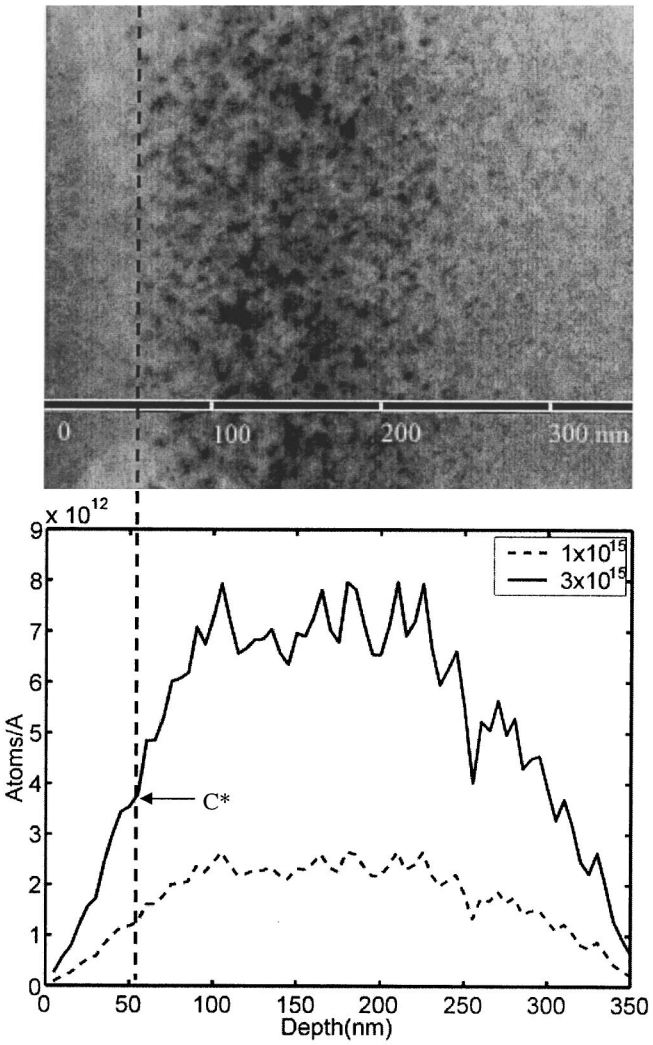

FIG. 6. Cross-sectional TEM bright field micrograph of a Si sample implanted to $3\times10^{15}/\mathrm{cm}^2$. The lower figure shows the Si ion distributions of two doses, $1\times10^{15}/\mathrm{cm}^2$ (dashed line) and $3\times10^{15}/\mathrm{cm}^2$ (solid line) from TRIM simulations. The dotted line illustrates the region where the visible threshold takes effect. C^* is the defect concentration at the threshold dose.

although highly damaged by the implantation beam, is notably denuded of visible defects. Comparison of the visible damage zone with the implantation profiles in Fig. 6 indicates that dislocations form when the implanted concentration of interstitials exceeds $\approx1\times10^{-3}$ atom fraction.

B. Evolution of defect structure during isochronal annealing

HDS measurements were performed on the irradiated samples discussed in Sec. III A, following annealing to elevated temperatures. The primary results are shown in Fig. 7(a) and 7(b) where Iq^2 is plotted as a function of temperature for the different implanted samples. In Fig. 7(a) all of the data are plotted on the same scale to illustrate the relative magnitudes of the scattering, while in Fig. 7(b), the data are plotted to show the fractional change in the scattering as a function of temperature. A few systematic trends are clearly observable in these data. For the samples containing lowest three doses, the scattering decreases significantly upon annealing at $\approx400\,^\circ$C. For the two other samples, such annealing is not observed, or it is small. Between 400 and 700 °C, the annealing continues in the two samples with the lowest doses, whereas very little change, or even a small increase, in the scattering is observed in the specimens implanted to the highest doses.

On further annealing to $\approx875\,^\circ$C, all samples, except the one with the lowest dose, show a marked increase in scattering. For the three samples with the highest dose, the scattering at this point in the isochronal anneal is, in fact, larger than the values immediately after implantation at 100 °C. On the other hand, the change in scattering intensity at its peak, relative to that at its minimum, $\approx700\,^\circ$C, is largest for the samples irradiated to 3 and 10×10^{14} cm^{-2} and smallest for the sample irradiated to the highest dose. Unfortunately the sensitivity is not sufficient to determine if there is a corresponding increase in intensity for the sample irradiated to the lowest dose. Relative to the initial scattering, however, any such peak in this sample would be small in comparison to the other specimens.

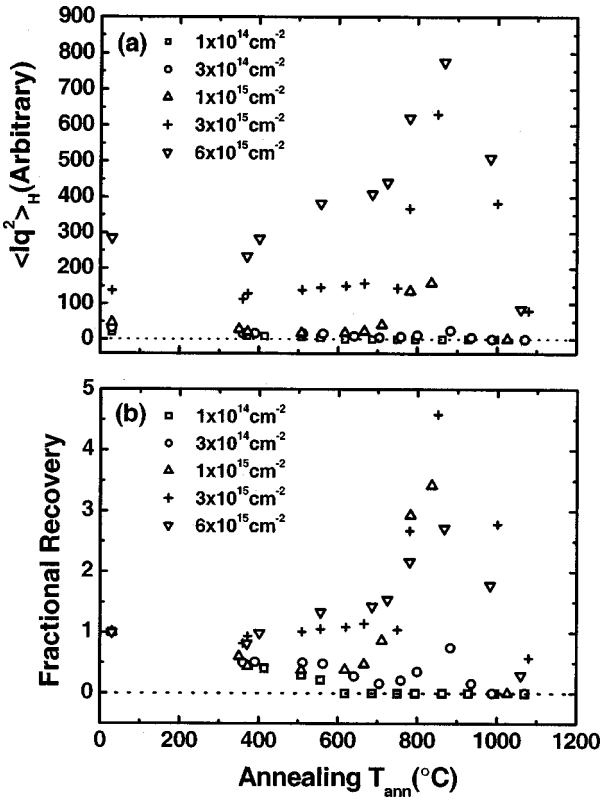

FIG. 7. Average Iq^2 of HDS measurements, $\langle Iq^2\rangle_H$, as a function of annealing temperature. (a) The data are plotted on the same scale to illustrate the relative magnitudes. (b) The recovery ratio, $\langle Iq^2\rangle_T/\langle Iq^2\rangle_{T=100°C}$, as a function of annealing temperature.

Since we attribute the increase in intensity during annealing to the clustering of defects, we have also considered the asymmetry of the scattering. We define the asymmetry as the ratio of scattering as, $A=(\langle Iq^2\rangle_q-\langle Iq^2\rangle_{-q})/(\langle Iq^2\rangle_q+\langle Iq^2\rangle_{-q})$ and plot it as a function of temperature for four samples in Fig. 8. Again, systematic trends are observed. The two samples irradiated to lowest doses show a large peak in asymmetry $\approx$600 °C, whereas the asymmetry in the samples irradiated to the highest show only small changes at this temperature. Note, a positive value of A represents scattering predominantly from interstitial defects and a negative value indicates vacancy defects, so that in all cases, the scattering is mostly from interstitials. Expected values of the anisotropy for different types of defects are listed in Table I. Values for interstitials loops derive from the calculations of Nordlund[24] and Ehrhart,[11] while those for the point defect clusters were obtained by calculating the diffuse scattering for the displacement fields given in Ref. 25. Our method for calculating the diffuse scattering has been described elsewhere.[26]

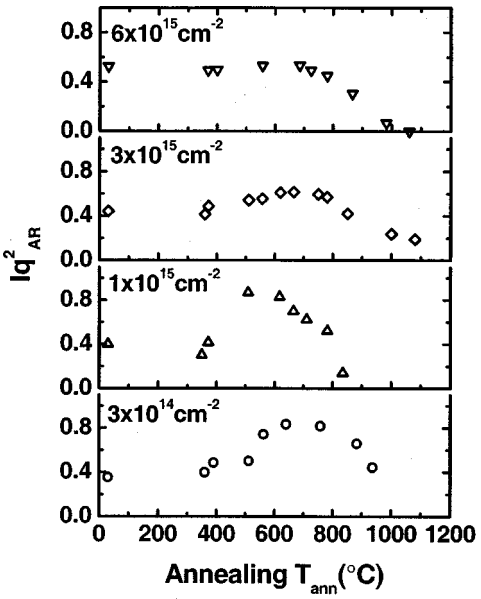

FIG. 8. Asymmetry of HDS, Iq_2^{AR}, as a function of annealing temperature for samples implanted with various doses.

IV. DISCUSSION

A. Dependence of defect structure on dose during implantation

The integrated strain, plotted in Fig. 5(c) is a direct measure of the sum of the relaxation volumes of all defects in the sample, i.e.,

$$\varepsilon_z = \sum c_i F \Delta V_i, \tag{1}$$

where the sum on "i" is over all defect types, c_i is the concentration of defect "i," ΔV_i is the relaxation volume of the defect (in units of atomic volumes), and F is a factor related to the elastic constants. Although the dependence of the Huang scattering on defect concentration is more complex, it is plotted in Fig. 5(c) for comparison. The two sets of data are qualitatively similar. Extrapolation of both sets of data in the low dose regime to zero dose shows that neither goes through zero. Since both the HDS and strain are zero prior to irradiation, the data simply imply that the damage increases very quickly with dose at low doses, below 1×10^{14} cm^{-2} and then it tends to saturate at the end of the low-dose regime, before increasing again in the high-dose regime.

Saturation behavior is a commonly observed feature in irradiated materials and is due to recombination reactions between vacancies and interstitials and their clusters. The saturation concentration of defects depends on a number of factors, including the type of ion used for irradiation and its

TABLE I. Anisotropy for various defect structures from the theoretical calculations. The data of interstitials and vacancies are from Ref. 25. The data of (111) loops are from reference [11] and the data of (311) loops are from Ref. 24.

Type of defect	1-interstitial	2-interstitial	4-interstitial	1-vacancy	3-vacancy
Anisotropy	0.74	0.54	0.42	−0.62.	−0.57
Type of loop	(111) perfect	(311) hex	(311) IRD		
Anisotropy	0.75	0.73	0.54		

energy, the irradiation temperature, and, of course, the target material. For Si irradiated with self-ions at room temperature, the dose required for saturation exceeds that required for amorphization, and so its value is not known. At higher temperatures the saturation concentration is reduced, and in Si this reduction is clearly sufficient at 100 °C to prevent amorphization. In metals[27] and AlAs,[28] saturation concentration of defects is $\approx 5\times10^{-3}$.

While the defect concentration at saturation cannot be determined accurately from the present experiment, we can provide a rough estimate by assuming that each Frenkel pair has a relaxation volume of $\approx 1\Omega_o$. Thus, using Eq. (1) and noting that the average strain at the saturation dose ($\approx 3\times10^{14}$ cm^{-2}) is $\approx 5\times10^{-4}$, we obtain a defect concentration on the order of 1×10^{-3}. This value is well below that required for amorphization, $\approx 5\times10^{-2}$, which we have estimated by the same means using the strain data from Refs. 21 and 29. It is noteworthy that at the dose signaling the onset of regime II, $\phi_0^{II}\approx 1\times10^{15}$ cm^{-2}, the concentration of implanted Si atoms also is $c_{Si}=5\times10^{-4}$, (see Fig. 6). Since the relaxation volume of the added Si atom, i.e., an interstitial, is approximately equal to the relaxation volume of the Frenkel pair, the concentration of Frenkel pairs after a dose of 3×10^{14} cm^{-2}, i.e. at saturation, must also be $\approx 5\times10^{-4}$ agreeing well with our estimate above. These results thus suggest that the creation of strain in region I is due to the creation of Frenkel pairs, and that this process saturates. Eventually, the concentration of implanted Si exceeds the Frenkel pair concentration, marking the beginning of region II, and that strain then builds by the simple addition of implanted Si atoms.

We can make these ideas more quantitative by noting from the TEM results that at doses $\approx 1-3\times10^{15}$ cm^{-2}, the defects collapse into dislocation loops. From the results of the Huang scattering, and the discussion above concerning the origin of the strain in region II, we can reasonably assume that the loops are interstitial in character. The relaxation volume of interstitials atoms in loops must be very nearly $1\Omega_o$, and thus the uncertainty in the relaxation volume of defect clusters encountered in the above qualitative discussion is now eliminated. The strain arising from implanted Si atoms, therefore, can be simply obtained as follows. Notice first, however, that since the near-surface region is constrained in the plane of the surface, an interstitial atom causes dilation in only the z direction, and it is given by

$$\varepsilon_z = \varepsilon_{zo} + \frac{\nu}{1-\nu}(\varepsilon_{xo} + \varepsilon_{yo}), \tag{2}$$

where ε_z is the strain on the direction normal to the surface, z; ν is the Poisson's ratio; ε_{x0}, ε_{y0}, and ε_{z0} are the strains in an isotropic unconstrained system when an interstitial is added and given by

$$\varepsilon_{xo} = \varepsilon_{yo} = \varepsilon_{zo} = \frac{1}{3}\cdot\frac{\Delta V}{V}, \tag{3}$$

where ΔV is the volume change due to an added atom, and when added to dislocation loops, $\Delta V=\Omega_0$. Poisson's ratio is 0.20 for the [111] direction.[30] Thus, combining these values in Eq. (2) yields,

$$\varepsilon_z = 0.41\phi\frac{\Delta V}{V} \tag{4}$$

where ϕ is the ion dose in units of cm^{-2}. Comparison of the calculated strain due to the addition of interstitials with the experimental strains in Fig. 5(c) shows that at low doses the strain is larger than that expected from simply adding interstitials, while at high doses the added interstitials can account for nearly all of the strain (within uncertainties in the volume per defect, the irradiated volume, and the strain measurements). The calculated curve in this figure was obtained by superposing the strain arising from the Frenkel pairs created at low dose with that due to implanted Si atoms, Eq. (4). The strain arising from the implanted Si atoms equals that from the Frenkel pairs at a dose of $\approx 1\times10^{15}$ cm^{-2}. We can conclude therefore, that the defects state in Si changes during implantation, from one consisting of small clusters of interstitials and vacancies below 1×10^{15} cm^{-2}, to one comprised predominantly of interstitial loops above it. Moreover, the loops grow in the high-dose regime according to one interstitial per implanted ion, i.e., the so-called "plus one" model is well obeyed in this regime.

B. Dependence of defect structure on annealing temperature

The measurements of Huang scattering during isochronal annealing can be largely understood in terms of the defect state existing at the end of the implantation at 100 °C. For the doses falling within region I, $\phi<1\times10^{15}$ cm^{-2}, the defects are primarily in the form of small interstitial and vacancy clusters, with the total concentrations of vacancies and interstitials being nearly equal. Since di-interstitial and divacancies and higher order clusters are not mobile at this temperature[31] and do not dissociate, the sizes of these clusters must be small.[32] On annealing to 400 and 700 °C, these small vacancy and interstitial clusters either become mobile or dissociate and undergo recombination reactions with their annihilation partners, although the growth of clusters is also possible. Until the clusters reach a size where they become immobile, or stable against dissociation, recombination reactions will continue. This leads to substantial recovery in the Huang scattering for the specimens irradiated to low doses. For the specimen implanted with doses in region II, the concentration of interstitials is far larger than that of vacancies, thus limiting the amount of recombination possible. In addition, the interstitial clusters have mostly formed dislocation configurations in region II, at the implantation temperature, and thus they are stable against dissociation until much higher temperatures. Thus, little recovery in the Huang scattering is observed on annealing to 700 °C.

For annealing above 700 °C it has been observed on specimens irradiated at room temperature to doses less that $\approx 5\times10^{13}$ cm^{-2}, that dislocations begin to form.[6] For these "low-dose" experiments, this has been explained by the dissociation of interstitial clusters containing four interstitials and their subsequent migration and formation of even larger clusters and eventually dislocations.[32] The present experiments can be understood in similar terms, although the initial

defect concentration must be taken into account to understand the details. For the sample implanted to the lowest dose, for example, Fig. 7(b) shows that fraction of Huang scattering remaining is very small above 700 °C, although there is some indication of a small peak. This peak becomes far more prominent for the sample irradiated to a dose of 3×10^{14} cm^{-2}. While the defect concentration cannot be increasing during annealing, the scattering from clusters increases with their size, approximately as the square of the number of interstitials in the cluster for three dimensional defect clusters. Consequently the total scattering increases as the defects cluster further and not too many defects annihilate. For the sample implanted to a dose of 3×10^{14} cm^{-2}, which is in region I, both reactions take place, but the clustering reaction prevails between 800 and 900 °C when most vacancies have already been annihilated and interstitial clusters grow rapidly.

The samples irradiated to 1×10^{15} and 3×10^{15} cm^{-2} represent the onset of region II, in terms of dose, such that there is already a large excess of interstitials compared to vacancies prior to annealing. Recombination of defects, in these samples, therefore, is very much limited above 700 °C. As a consequence, the peaks in the scattering intensity at $\approx$850 °C are very large as the interstitial clusters grow in size without the competing recombination reaction. For the sample irradiated to the highest dose, increases in scattering are also observed, but it is less pronounced than that for the specimens irradiated to 1×10^{15} and 3×10^{15} cm^{-2}, even though the remaining numbers of vacancies above 700 °C in this sample is negligible. Most of the interstitial defects in this sample, however, are in the form of dislocations following the implantation at 100 °C. As a consequence there are relatively few small defect clusters that can grow on annealing above 700 °C. Moreover, once the defects form dislocations, the scattering is no longer Huang scattering, but rather it falls in the asymptotic scattering regime. This scattering is proportional to the absolute concentration of defects and is independent of the size of the defects. Thus, even if some growth in the size of the dislocations were to occur, the scattering would be relatively insensitive to these changes. The total scattering in this sample, however, remains larger than in the other samples; it is only the relative changes in the scattering that are small. Above 900 °C, the interstitial loops dissolve and complete recovery in all samples takes place.

V. CONCLUSIONS

The development of the defect structure in Si implanted with self-ions to high doses was investigated using x-ray scattering and TEM, both as a function of dose and during subsequent isochronal annealing. By implanting at 100 °C, high implantation doses could be employed without causing amorphization. Two regimes in the damage production were observed. Below $\approx1\times10^{15}$ cm^{-2}, the damage defect state contained both vacancies and interstitials, and in approximately equal numbers. The number of implanted interstitials was small compared to the number produced by the implantation, even though both vacancies and interstitials were mobile at the implantation temperature. After a dose $a\approx3\times10^{14}$ cm^{-2}, the defect concentration arising from damage production during implantation tended to saturate at a concentration of $\approx1\times10^{-3}$, which is far below that required for amorphization in Si.

At a dose of $\approx1\times10^{15}$ cm^{-2}, the concentration of implanted Si atoms became comparable to the saturation concentration of Frenkel pairs, causing a profound difference in the defect state. Since the concentration of Frenkel pairs had saturated, the interstitial clusters began to dominate the defect state. Their growth eventually led to the formation of dislocations with interstitial character. In this implantation regime, the "plus-one" model for defect production was well obeyed.

The annealing behavior reflected the initial state of damage within the implanted Si samples. At low doses, the concentrations of interstitials and vacancies were very similar, and substantial recovery was observed below 600 °C. As the dose was increased, the imbalance in vacancies and interstitials grew, restricting the recombination reaction and enabling the interstitial clusters to grow to large sizes and eventually form dislocations. At the highest doses, 3×10^{15} cm^{-2}, and above, the imbalance in vacancy and interstitial concentration was very large, and this suppressed the amount of recovery arising from recombination. Since the interstitials clusters were already in the form of dislocations at the implantation temperature, the growth of small clusters was also suppressed. Finally, above $\approx$900 °C, the interstitial clusters began to shrink, either by recombination with thermal vacancies or by dissolution and loss to sinks.

ACKNOWLEDGMENTS

This research was supported by National Science Foundation, under Grant No. DMR-9986160, and in part by a MURI Grant No. F49620-01-1-0336. The X16A beamline at NSLS and the CMM are operated by the UIUC Materials Research Laboaratory, and are supported by the U.S. Department of Energy (DOE) under Grant No. DEFG02-91ER45439. The NSLS is operated by the DOE under Grant No. DEAC02-98CH10886. The authors are grateful to Dr. P. Ehrhart for critical comments concerning the interpretation of the x-ray scattering results. The authors are grateful to Dr. L. Funk and P. Baldo for performing the ion implantations. C. J. B. acknowledges the Swiss National Science Foundation for the financial support.

APPENDIX: KINEMATICAL SIMULATION OF ROCKING CURVES

In constructing a scattering model to analyze our results, we assume that the strain follows a Gaussian distribution,

$$\varepsilon(z) = A\,\exp\left[\frac{(z-z_0)^2}{2\sigma^2}\right], \tag{A1}$$

where $\varepsilon(z)$ is the fractional layer expansion of the average crystal at depth z increasing inwards from the surface at $z=0$. This is a good approximation to the numerical distributions found in previous studies.[21] The characteristic offset of the distribution from the surface is represented by z_0. The

fractional amplitude A provides the total magnitude of the strain.

Since closed-form analytical expressions are difficult to derive, even in the kinematical limit, we used a one-dimensional numerical expression to calculate the diffraction profiles. The structure factor $F(q)$ representing the diffracted beam at reciprocal lattice coordinate q is given in this one dimensional kinematical model by,

$$F(q) = f_0 \sum_{j=-\infty}^{N} e^{iqz}j = f_0 \sum_{j=-\infty}^{0} e^{iqaj} + f_0 \sum_{j=1}^{N} e^{iqz_j} = \frac{f_0}{1 - e^{-iqa}} + f_0 \sum_{j=1}^{N} e^{iqz_j}. \quad \text{(A2)}$$

The infinite sum over the layers of the crystal at location z_j has been split into an unstrained region and one in which the strain is considered to be positive. The unstrained bulk lattice spacing is a. The analytical sum is evaluated in the (infinite) unstrained region in the form of a CTR,[23] while the contribution of the strained region from $j=1$ to N is evaluated explicitly. The numerical cutoff parameter N was chosen simply so that the sum begins sufficiently deep in the crystal that the exponential tail of the strain distribution in Eq. (A1) does not affect the result. In the latter region, the layer positions are determined by the recursion relations,

$$z_1 = a$$

$$z_j = z_{j-1} + a\{1 + \varepsilon[(N-j)\dot{a}]\}. \quad \text{(A3)}$$

The intensity $|F(q)|^2$ calculated using the functional form of Eq. (A2) gives good fits to the rocking curve measurements but with one modification. The form of Eq. (A2) slightly overemphasizes the amplitude of the intensity oscillations, especially at larger strains, but it does predict the positions of the maxima and minima correctly. The modified form includes weights of the contributions to the structure factor from the layers in the strained region,

$$F(q) = \frac{f_0}{1 - e^{-iqaj}} + f_0 \sum_{j=1}^{N} W[(N-j)a]e^{iqazj}, \quad \text{(A4)}$$

where $W(z)$ is the weighting of the layers at depth $z=(N-j)a$. A similar weighting function was found to be useful by Milita and Servidori.[19,22] Different forms of $W(z)$ were tried and satisfactory results were obtained by linking the weighting function directly to the (Gaussian) strain distribution function itself,

$$W(z) = 1 - \alpha\varepsilon(z) \quad \text{(A5)}$$

where α is a an additional fitting parameter. The physical meaning of Eq. (A5) is that the layers with the most strain contribute proportionally less to the structure factor in Eq. (A4); thus it is similar to a static Debye-Waller factor, representing the disorder of the lattice. Whereas the strain profile of Eq. (A1) designates the *average* position of the crystal layers, the actual positions of the atoms within those layers will be redistributed by the damage induced by the local strain associated with the point defects. Within this Debye-Waller picture, the net contribution to the diffraction of each partly disordered layer is thereby reduced and so can be modeled by a single layer with reduced occupancy at the average position.

[1] See, e.g., G. D. Watkins, *Electronic Structure and Properties of Semiconductors, Materials Science and Technology*, Vol. 4 edited by W. Schroeter, (VCH, Weinheim, 1991).
[2] S. Bagchi, S. J. Krause, and P. Roitman, Appl. Phys. Lett. **71**, 2136 (1997).
[3] A. P. Knights, G. R. Carlow, M. Zinke-Allmang, and P. J. Simpson, Phys. Rev. B **54**, 13955 (1996).
[4] S. Krause, M. Anc, and P. Roitman, MRS Bull. **23**, 15 (1998).
[5] A. Agarwal *et al.*, Appl. Phys. Lett. **70**, 3332 (1997).
[6] J. L. Benton, S. Libertino, P. Kringhioj, D. J. Eaglesham, J. M. Poate, and S. Coffa, J. Appl. Phys. **82**, 120 (1997).
[7] R. Kalyanaraman, T. E. Haynes, O. W. Holland, H-J. L. Gossmann, C. S. Rafferty, and G. H. Gilmer, Appl. Phys. Lett. **79**, 1983 (2001).
[8] See, e.g., S. Grotehans, G. Wallner, E. Burkel, H. Metzger, J. Peisl, and H. Wagner, Phys. Rev. B **39**, 8450 (1989).
[9] I. K. Robinson and D. J. Tweet, Rep. Prog. Phys. **55**, 599 (1992).
[10] P. H. Dederichs, J. Phys. F: Met. Phys. **3**, 471 (1973).
[11] P. Ehrhart, J. Nucl. Mater. **216**, 170 (1994).
[12] M. A. Krivoglaz, *Theory of X-ray and Thermal-Neutron Scattering by Real Crystals* (Plenum, New York, 1969).
[13] U. Beck, T. H. Metzger, J. Peisl, and J. R. Patel, Appl. Phys. Lett. **76**, 2698 (2000).
[14] P. Partyka, Y. Zhong, K. Nordlund, R. S. Averback, I. K. Robinson, and P. Ehrhart, Phys. Rev. B **64**, 235207 (2001).
[15] C. J. Tsai, A. Dommann, M. A. Nicolet, and T. Vreeland, J. Appl. Phys. **69**, 2076 (1991).
[16] C. J. Tsai, T. Vreeland, and H. A. Atwater, Appl. Phys. Lett. **64**, 434 (1994).
[17] B. M. Paine, N. N. Hurvitz, and V. S. Speriosu, J. Appl. Phys. **61**, 1335 (1987).
[18] C. A. Cima, H. Boudinov, J. P. de Souza, Y. Suprun-Belevich, and P. F. P. Fichter, J. Appl. Phys. **88**, 1771 (2000).
[19] S. Milita and M. Servidori, J. Appl. Phys. **79**, 8278 (1996).
[20] A. Pesek, P. Kastler, L. Palmetshofer, F. Hauzenberger. P. Juza, W. Faschinger, and K. Lischka, J. Phys. D **26**, A177 (1993).
[21] V. S. Speriosu, B. M. Paine, M-A. Nicolet, and H. L. Glass, Appl. Phys. Lett. **40**, 604 (1982).
[22] D. K. Bowen and B. K. Tanner, *High Resolution X-ray Diffractometry and Topography* (Taylor & Francis, London, 1998).
[23] I. K. Robinson, Phys. Rev. B **33**, 3830 (1986).
[24] K. Nordlund, J. Appl. Phys. **91**, 2978 (2002).
[25] K. Nordlund, P. Partyka, R. S. Averback, I. K. Robinson, and P. Ehrhart, J. Appl. Phys. **88**, 2278 (2000).
[26] K. Nordlund, P. Partyka, and R. S. Averback, Mater. Res. Soc. Symp. Proc. **469**, 199 (1997).
[27] See, e.g., H. J. Wollenberger, in *Vacancies and Interstitials in Metals*, edited by A. Seeger, D. Schumacher, W. Schilling, and J. Diehl (North Holland, Amsterdam, 1970), p. 215.
[28] P. Partyka, R. S. Averback, D. V. Forbes, J. J. Coleman, P. Ehrhart, and W. J. Jager, Appl. Phys. Lett. **65**, 421 (1994).
[29] G. Bai and M.-A. Nicolet, J. Appl. Phys. **70**, 649 (1991).
[30] J. J. Wortman and R. A. Evans, J. Appl. Phys. **36**, 153 (1965).
[31] C. Christofids, Semicond. Sci. Technol. **7**, 1283 (1992).
[32] N. E. B. Cowern *et al.*, Phys. Rev. Lett. **82**, 4460 (1999).